A model of the Earth's Dole effect

Georg Hoffmann,[1,2] Matthias Cuntz,[1,2] Christine Weber,[3] Philippe Ciais,[1,2] Pierre Friedlingstein,[1,2] Martin Heimann,[4] Jean Jouzel,[1,2] Jörg Kaduk,[5] Ernst Maier-Reimer,[3] Ulrike Seibt,[4] and Katharina Six[3]

[1]   The Earth's Dole effect describes the isotopic $^{18}O/^{16}O$-enrichment of atmospheric oxygen with respect to ocean water, amounting under today's conditions to 23.5‰. We have developed a model of the Earth's Dole effect by combining the results of three-dimensional models of the oceanic and terrestrial carbon and oxygen cycles with results of atmospheric general circulation models (AGCMs) with built-in water isotope diagnostics. We obtain a range from 22.4‰ to 23.3‰ for the isotopic enrichment of atmospheric oxygen. We estimate a stronger contribution to the global Dole effect by the terrestrial relative to the marine biosphere in contrast to previous studies. This is primarily caused by a modeled high leaf water enrichment of 5−6‰. Leaf water enrichment rises by ∼1‰ to 6−7‰ when we use it to fit the observed 23.5‰ of the global Dole effect. The present model is designed to be utilized in forthcoming paleo studies allowing a quantitative analysis of long-term observations from polar ice cores.   *INDEX TERMS:* 0330 Atmospheric Composition and Structure: Geochemical cycles; 1040 Geochemistry: Isotopic composition/ chemistry; 1610 Global Change: Atmosphere (0315, 0325); 1854 Hydrology: Precipitation (3354); *KEYWORDS:* carbon cycle, Dole effect, water isotopes

1.   Introduction

[2]   The Dole effect (DE in the following), i.e., the isotopic $^{18}O/^{16}O$-enrichment of atmospheric oxygen with respect to ocean water, is affected by a number of different processes in the global cycle of molecular oxygen and of water: strength and type of terrestrial and marine oxygen fluxes, evapotranspiration, and humidity over the continents [*Bender et al.*, 1994b]. Modeling of the DE is therefore a valuable test case of Earth system models which integrate biological and climatic components. Furthermore, variations of the DE in the Quaternary have large implications for the interpretation and dating of polar ice cores [*Bender et al.*, 1994a, 1994b; *Jouzel et al.*, 2002; *Shackleton*, 2000]. A prognostic model of the DE therefore will help to identify the relevant forcing factors affecting the DE in the past.

[3]   Measurements of the isotopic composition of a number of bioactive atmospheric gases were used to better separate and quantify the natural and anthropogenic perturbation of the global cycles of carbon and oxygen [*Keeling*, 1960, 1995]. Because of the integrating tendency of the atmosphere, this approach avoids the problem of deducing general information from spatially and temporally highly variable local measurements. For example, the carbon isotopic composition of CO2 has been used to separate marine and terrestrial sources [*Ciais et al.*, 1995] and the oxygen isotopic relation of CO_2, $C^{18}O^{16}O/C^{16}O_2$, to separate the gross exchange fluxes of terrestrial ecosystems [*Ciais et al.*, 1997a, 1997b; *Farquhar et al.*, 1993; *Peylin et al.*, 1999]. The $^{18}O/^{16}O$ oxygen, $\delta^{18}O_{Atm}$, has up to now primarily been used in paleoclimatic studies [*Bender et al.*, 1994a, 1994b; *Sowers et al.*, 1991]. The long atmospheric residence time of oxygen of approximately 1200 years [*Bender et al.*, 1994b], and the fact that within today's measuring precision no interhemispheric gradient has been detected, make the $\delta^{18}O_{Atm}$ signal an interesting tool to synchronize Northern and Southern Hemispheric ice core records. Similar to the oxygen isotopic tracer of CO_2, $\delta^{18}O_{Atm}$ is strongly affected by photosynthesis and respiration in the carbon/oxygen cycle and by the hydrological cycle. The enrichment of today's atmospheric oxygen of 23.5‰ Vienna- Standard Mean Ocean Water (V-SMOW) [see *Craig*, 1961] relative to its largest source, the global oceans, was called the Dole effect [*Dole*, 1935; *Morita and Titani*, 1936]. Similar to the isotopic tracers of carbon dioxide ($^{13}CO_2$, $C^{18}O^{16}O$), spatial and temporal variations of $\delta^{18}O_{Atm}$ must exist, however, because of the large atmospheric abundance of oxygen, these are expected to be very small and have not been observed in modern air samples until now. It will need at least 1 order of magnitude higher precision of modern mass spectrometric techniques

[1]Institut Pierre Simon Laplace (IPSL), Paris, France.
[2]Also at Laboratoire des Sciences du Climat et de l'Environnement (LSCE), Orme des Merisiers, Gif sur Yvette, France.
[3]Max-Planck-Institut für Meteorologie, Hamburg, Germany.
[4]Max-Planck-Institut für Biogeochemie, Jena, Germany.
[5]Department of Geography, University of Leicester, England, UK.

for measuring such variations. However, air bubbles enclosed in ice samples from polar ice cores exhibit deviations from the modern value of up to 0.7‰ [*Bender et al.*, 1994b; *Malaize et al.*, 1999; *Sowers et al.*, 1991], demonstrating drastic changes in the carbon or/and the hydrological cycle in the past.

[4] We present here a prognostic model of the DE based on the output of spatially and temporally resolved biochemical models of the O_2 cycle. These models include built-in diagnostic modules for calculating the various isotope fractionations as a function of local climate conditions. Former highly parameterized modeling efforts to understand the DE and its variations in the past focused on the sensitivity of the calculation to the various assumptions applied [*Leuenberger*, 1997]. In contrast, the model presented here provides a process-based approach for inferring the DE. It estimates today's and past DE from first principles solely as a consequence of the corresponding climate conditions.

[5] Section 2 reviews the present understanding of the processes controlling the DE. In section 3 we present the model components and discuss in detail the methods utilized to combine model results and to estimate the DE in this study. We next focus in section 4 on the spatial signature of the result and the uncertainties in the model. Finally, we conclude with a discussion of possible applications of the model to learn about long-term changes of the DE during the Pleistocene and what follows in the future.

2. Dole Effect

[6] *Bender et al.* [1994b] reviewed the progress that has been made in the last 15 years to better estimate the various fractionation processes of the oxygen isotopes and calculated a global balance of the different sources and sinks of ^{18}O of atmospheric oxygen. Figure 1 shows in a schematic way the results of *Bender et al.* [1994b] based on their estimated O_2 fluxes and fractionation coefficients (see also Table 1). Respiration represents a variety of processes, which oxidize organic carbon and release CO_2 while consuming molecular O_2. During respirative consumption of oxygen, most of the O_2 sink components are accompanied by a fractionation of approximately 20‰. In the terrestrial domain a more or less direct exchange of the consumed oxygen with the atmospheric reservoir takes place. Dissolved oxygen, O_{2DISS}, in the deep ocean, however, represents an oxygen pool that exchanges with the atmosphere solely on the long timescale of oceanic deep water circulation (100 to 1000 years). Respirative fractionation therefore enriches O_{2DISS} considerably, particularly in oceanic regions with high remineralization rates and comparably low exchange rates with the surface ocean and the overlying atmosphere. $\delta^{18}O_{DISS}$ denotes the $^{18}O/^{16}O$-relation in δ-notation of dissolved oxygen, O_{2DISS}. The $\delta^{18}O_{DISS}$ is enriched by as much as 15‰ relative to the atmospheric signal, that means 38‰ relative to V-SMOW [*Kroopnick*, 1987]. As a consequence, the contribution of mineralization in the deep ocean to the atmospheric DE decreases its value, with an asymptotic value of 12‰ [*Bender et al.*, 1994b]. The larger part (about 95%) of oceanic respiration, however,

takes place in the euphotic layer where dissolved O_2 has a residence time of a few weeks and therefore is in close isotopic equilibrium with the atmosphere. Here the respirative fractionation was estimated, similar to the terrestrial environment, to be 20‰. Summarizing the role of respiration in controlling the DE, Bender et al. concluded that land or ocean respiration alone cannot explain the observed high value of 23.5‰ (respiration effects sum up to 18.8‰) and that in the terrestrial and the marine biosphere, respiratory fractionation is about equally strong.

[7] In vitro experiments of *Guy et al.* [1993] demonstrated that during the photosynthetic production of O_2, there is no additional fractionation relative to the water from which the oxygen isotopes originate. For the marine domain, therefore, photosynthesis is a source of O_2 being in equilibrium with the isotopic composition of water in the euphotic zone. From early water isotope measurements, it has long been known that ocean surface water varies typically between −1.5‰ in polar regions to + 0.5‰ in the tropics [*Craig and Gordon*, 1965; *Schmidt*, 1999]. The area-weighted global average is close to 0‰, which is thus a good estimate for the isotopic composition of the oxygen released during photosynthetic activity of plankton. In the terrestrial environment, the water surrounding the biochemical diagenesis of oxygen is strongly enriched by evapotranspiration from leaves. Plant transpiration correlates with photosynthetic O_2 emissions to the atmosphere. Water taken up by the roots is transpired through the leaves. During evaporation and diffusion through the stomata and through the leaf boundary layer, an enrichment of the remaining leaf water takes place. According to different studies, this enrichment amounts to a global production-weighted average of between +4−+8‰ [*Dongmann*, 1974; *Farquhar et al.*, 1993]. This enrichment of leaf water depends on a number of factors, some of them are "external" to the plants. For example, the rainout of air masses affects the isotopic composition of the soil water taken up by the plants, or relative humidity close to the stomata controls the balance between evaporation and diffusion out of the stomata. It also depends on "internal" processes, such as the mixing between depleted sapwater and enriched evaporative water within the leaves. The terrestrial $^{18}O^{16}O$ flux therefore is strongly influenced both by the external boundary condition imposed by water isotope physics and by internal processes affecting the turnover of water in leaves. Anthropogenic combustion processes, accompanied by fractionation as well, were not considered assuming that today's DE has not yet been altered by them to measurable extent. The budget presented here therefore primarily reflects pre-industrial conditions.

[8] To calculate the DE, *Bender et al.* [1994b] sum up the different fractionation factors discussed above weighted with the respective oxygen fluxes. Owing to the considerable (more than 4‰) difference between the oceanic and the terrestrial contribution to the global DE, the relation between the respective production rates (annual turnover of moles of O_2), P_O for the ocean and P_T for the terrestrial environment, is crucial in the calculation. It was estimated to $P_O/P_T \sim 1/2$. With these numbers the best guess of the global DE amounts to 20.4‰, considerably underestimating the observed value.
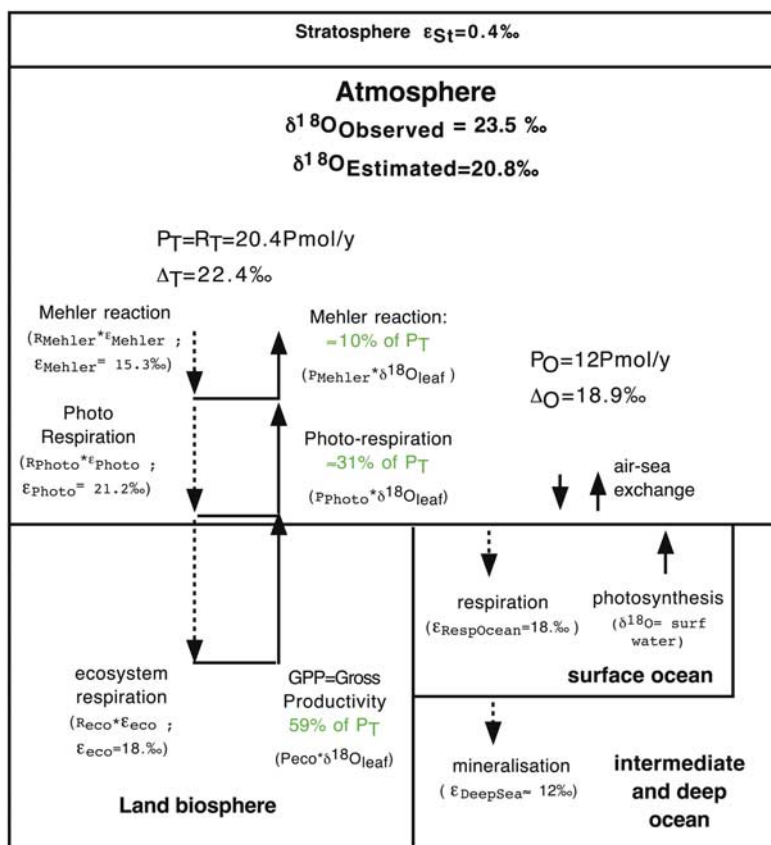
Figure 1. The global balance of the Dole effect according to *Bender et al.* [1994b]. Most notations correspond to those used in Tables 1 and 2; however, some numeric values are slightly different in this study (see citations in Table 2). Here $\varepsilon_{RespOcean}$ and $\varepsilon_{DeepSea}$ are the estimated ocean fractionation coefficients of *Bender et al.* [1994b]. They do not directly correspond to quantities in the study here since the ocean model calculates these quantities in an integrated way.

This gave rise to speculations that some important terms in the calculation might have been neglected, such as fractionation effects during the diffusion of oxygen in soils. However, the estimation is also accompanied by considerable uncertainties, the largest being the global isotopic composition of leaf water and the relative oxygen turnover rates in the terrestrial and the marine domain.

3. Model Construction

[9] The overall DE results (in the context of the following formulas we use the symbol Δ for the magnitude of the DE) from the combination of ocean processes of isotopic O_2 enrichment termed DO or "ocean Dole effect" and of the terrestrial equivalent DT, termed the "terrestrial Dole effect,"

$$\Delta = \delta^{18}O_{ATM} - \delta^{18}O_{OW} = F\Delta_O + (1 - F)\Delta_T - \varepsilon_{ST}, \quad (1)$$

with P_O and P_T being the O_2 fluxes of gross oceanic and terrestrial productivity, respectively, and the factor $F = P_O/$

Table 1. Budget of the DE According to This Study and *Bender et al.* [1994b][a]

	This Study	Bender et al.
Ocean production P_O, Pmol O_2/year	7.61	12.
Oceanic Dole effect Δ_O, ‰	16.97	18.90
Terr. Production P_T, Pmol O_2/year	16.7	20.4
Stdev, Pmol O_2/year	1.7	
Terrestrial Dole effect Δ_T, ‰	26.9 (25.9)	22.4
Stdev, ‰	0.3 (0.4)	
Relation P_O/P_T	0.45	0.59
Total Dole effect Δ, ‰	23.5 (22.9)	20.8
Stdev, ‰	0. (0.4)	
Observed Dole effect, ‰	23.5	

[a]All isotope values are given in ‰ deviation relative to VSMOW. For terrestrial effect values, the median and the corresponding standard variation of the three model simulations (ECHAM/SILVAN; ECHAM/SLAVE; GISS/SLAVE) are shown here. The values in brackets specify the values without correction for the diurnal effect (see text for details).
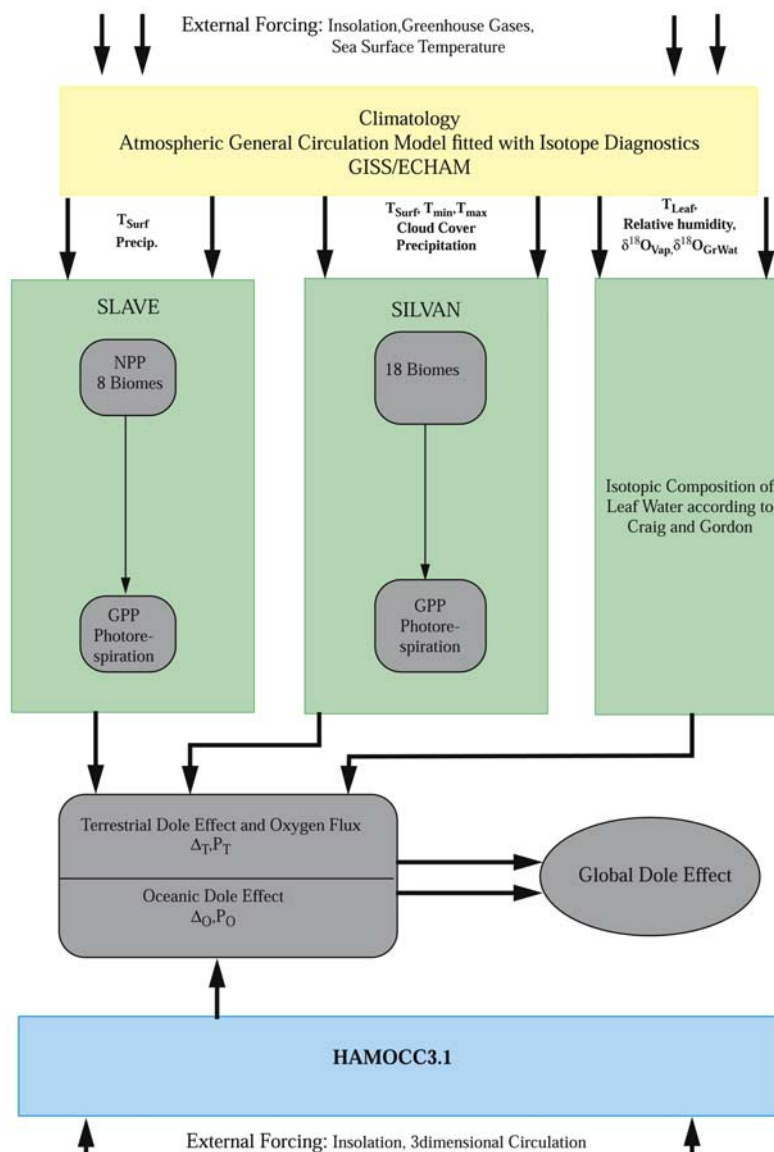
Figure 2. Information flux diagram for calculating the Dole effect. The terrestrial and the marine DE are estimated separately. For the terrestrial DE, a combination of two different AGCMs, GISS and ECHAM, and two different TBMs, SILVAN and SLAVE, are used. To calculate the modern O_2 Fluxes, both TBMs are forced with observed climatologies. In-line water isotope modules included in the two AGCMs infer the isotopic composition of precipitation and groundwater. The text discusses the results of the following model combinations: GISS + SLAVE, ECHAM + SLAVE and ECHAM + SILVAN. For the ocean part of the oxygen cycle, the ocean carbon cycle model HAMOCC3.1 is used, which calculates both the marine production, i.e., marine O_2 fluxes, and the isotopic equilibrium value in the atmosphere, i.e., the marine DE. The results of all three types of models are finally combined to calculate the Earth's Dole effect.

($P_O + P_T$). The term ε_{ST} is a small fractionation of 0.4‰ [*Bender et al.*, 1994b] due to an isotopic exchange between O_3 and CO_2 in the stratosphere. Respiratory uptake of O_2 preferentially consumes the light oxygen atoms ^{16}O, thus leaving the source oxygen reservoir isotopically enriched by approximately 20‰ depending on the type of respiration (see below). Photosynthetic production of O_2 releases oxygen isotopically labeled with the water surrounding the chloroplasts. In the ocean biosphere, this corresponds to the mean isotopic composition of water in the euphotic

layer, $\delta^{18}O_{EUPH}$. In the terrestrial domain, it corresponds to the isotope value of leaf water, $\delta^{18}O_{LEAF}$. It is mainly this evaporative enrichment, subsequently transferred onto atmospheric oxygen, that makes Δ_T larger than Δ_O. Because of this difference, a change in the relationship between the oceanic, P_O, and the terrestrial production rates, P_T, directly influences the DE.

[10] We estimate the terrestrial and the oceanic DE, Δ_T, and Δ_O, and the corresponding O_2 production rates, P_O and P_T, using a hierarchy of different models (Figure 2). The

estimate of Δ_T and P_T depends on the global distribution of $\delta^{18}O_{LEAF}$ and of the O_2 biotic exchange due to photosynthesis, photorespiration, and autotrophic and heterotrophic respiration. We deduce the modern $\delta^{18}O$ patterns in meteoric water from simulations with atmospheric general circulation models (AGCMs) with built-in modules for the computation of water isotopes. We have chosen observed climatologies, that is, temperature, precipitation, and cloud cover, in order to force the terrestrial biochemical models (TBMs).

3.1. Terrestrial Biosphere
3.1.1. Isotopic Composition of Leaf Water

[11] Two different AGCMs, the model of the Goddard Institute for Space Studies, GISS [*Hansen et al.*, 1983], and the model of the Max-Planck Institute for Meteorology, ECHAM3 [*Modellbetreuungsgruppe*, 1994], were integrated under modern climate boundary conditions. Both models simulate the water isotopes in vapor and precipitation by including specific fractionation processes between the various phases of water [*Hoffmann et al.*, 2000, 1998; *Jouzel et al.*, 1991, 1987]. The results of these simulations were extensively tested and validated against observations of water isotopes in precipitation which have been performed globally on a monthly basis by the International Atomic Energy Agency since more than 30 years [*International Atomic Energy Agency (IAEA)*, 1992; *Rozanski et al.*, 1992]. In summary, the modeled isotopic distribution has been found to be in excellent agreement with the observations, at least on the monthly to annual timescale considered here. From the modeled distribution of $\delta^{18}O$ in soil moisture and in near-groundwater vapor, we then estimated $\delta^{18}O_{LEAF}$ assuming steady state conditions during plant transpiration as described by the *Craig and Gordon* [1965] equation,

$$\delta^{18}O_{LEAF} = h \times \left(\delta^{18}O_{Vap} + \varepsilon_{EQUIL}\right) + (1 - h) \\ \times \left(\delta^{18}O_{GrWat} + \varepsilon_{EQUI}L - \varepsilon_{KIN}\right). \quad (2)$$

Here h denotes the relative humidity near the plant stomata, $\delta^{18}O_{Vap}$ and $\delta^{18}O_{GrWat}$ denote the ^{18}O content of vapor in the first model layer and of groundwater, respectively, ε_{EQUIL} describes the isotopic fractionation under equilibrium conditions ($\sim 10‰$, Table 2), and ε_{KIN} describes the strong kinetic fractionation during diffusive exchange of water molecules out of the stomata ($\sim -26‰$, Table 2). Typically, $\delta^{18}O_{GrWat}$ is about $10‰$ more enriched than $\delta^{18}O_{Vap}$. With the values given above, the difference between the first and the second term in the Craig and Gordon equation amounts to approximately $16‰$. Consequently, a larger h diminishes $\delta^{18}O_{LEAF}$; a lower h gives more weight to the kinetic fractionation and thus enhances $\delta^{18}O_{LEAF}$. Therefore, in this calculation, the specified relative humidity close to the plant stomata during daytime photosynthesis is crucial.

[12] Unfortunately, the employed monthly fields of relative humidity of both AGCMs are neither spatially nor temporally representative for the humidity within the canopy. First, the relative humidity is a prognostic variable calculated in the lowermost AGCM layer. This is at a height of about 30 m in the ECHAM model and at about 150 m in the GISS model. However, the relevant humidity in the *Craig and Gordon* [1965] formula (equation (2)) is the humidity at the leaf surface, which is normally higher than the humidity within the canopy or in the overlying free atmosphere. Second, and probably most important, over a daily cycle the relative humidity in the canopy undergoes large variations as does the isotopic composition of leaf water [*Bariac et al.*, 1994; *Förstel*, 1978]. In different forest types, daily amplitudes of $\delta^{18}O_{LEAF}$ of up to $10-15‰$ have been measured demonstrating the importance of computing $\delta^{18}O_{LEAF}$ synchronously with the daily cycle of O_2 fluxes. Moreover, the isotopic composition of sap water shows a large daily amplitude of about $2‰$. This is most probably due to an increasing pumping depth of the plant's root system during daytime when the demand of water for transpiration becomes larger [*Bariac et al.*, 1994]. Therefore $\delta^{18}O_{LEAF}$ (and thus the relative humidity) relevant for the O_2 fluxes has to be estimated during the photosynthetic activity of plants. The largest activity is typically observed close to sunlight maximum. However, physiological adaptations of plants avoiding large moisture losses at noon or climate conditions such as cloud coverage make the diurnal productivity cycle more complicate than a linear function of net incoming radiation [*Kim and Verma*, 1991]. A mechanistically correct computation of the isotopic composition of leaf water therefore would need a synchronous and detailed simulation of all these processes, which was not possible here. It was these uncertainties that lead *Bender et al.* [1994b] to conclude "that the biggest current uncertainty lies in the $\delta^{18}O$ of leaf water." Nevertheless, it seems reasonable to argue that the effective relative humidity relevant for the ^{18}O signal in the emitted O_2 must be considerably biased toward midday values which are typically lower than the monthly mean average.

[13] We try to correct here for the leaf temperature effect and the ignored daily cycle in a simple but consistent way. The monthly mean temperature of the AGCMs was corrected by an estimate of the daily temperature range (maximal-minimal temperature). Furthermore, we take into account the leaf temperature effect according to *Lloyd and Farquhar* [1994]. This procedure diminishes the calculated relative humidity by providing an effective leaf surface humidity and enhances the isotopic enrichment in the leaves. In detail, h is corrected by keeping the specific moisture content of the air constant and by modifying the corresponding temperature. The temperature, T, is enhanced proportional to the daily temperature range, i.e., $T_{Max} - T_{Min}$, by a factor γ, that is $T_{New} = T_{Old} + \gamma \times (T_{Max} - T_{Min})$. Leaf temperature is finally augmented by 5% according to *Lloyd and Farquhar* [1994], $T_{Leaf} = 1.05 \times T_{New}$. The relative humidity near the leaves and the isotopic enrichment of the leaf water is then calculated using this corrected air temperature T_{New} [*Seibt*, 1997]. In the three model combinations analyzed in this study (ECHAM/SLAVE, GISS/SLAVE, ECHAM/SILVAN), the globally averaged leaf water value, dLeaf, varied finally between 6.1 and 6.8‰ (before correction from 5.3‰ to 5.9‰). The factor γ represents the only real tuning parameter in our model of the DE. The value of γ was determined by matching the present-day global DE, yielding optimal values between

Table 2. List of Symbols Employed in the Text

Symbol	Definition
$\delta^{18}O_{ATM}$	$^{18}O/^{16}O$ isotopic composition of atmospheric oxygen
$\delta^{18}O_{OW}$	$^{18}O/^{16}O$ isotopic composition of mean ocean water
$\Delta = \delta^{18}O_{ATM} - \delta^{18}O_{OW}$	magnitude of the overall Dole effect
Δ_O	oceanic Dole effect
Δ_T	terrestrial Dole effect
ε_{ST}	= 0.4‰ stratospheric fractionation due to $O_2 - CO_2$ exchange [*Bender et al.*, 1994b]
P_O	marine O_2 production rates
P_T	terrestrial O_2 production rates, exactly balanced by the respiratory fluxes: R_{ECO}, R_{PHOTO} and R_{MEHLER}
$F = P_O/(P_O + P_T)$	relation of oceanic O_2 production to the total O_2 production
$\delta^{18}O_{EUPH}$	$\delta^{18}O$ of water in the euphotic layer of the ocean
$\delta^{18}O_{LEAF}$	$\delta^{18}O$ of water in the terrestrial biosphere (Leaves)
$\delta^{18}O_{GrWat}$	$\delta^{18}O$ of groundwater
$\delta^{18}O_{Vap}$	$\delta^{18}O$ of vapor in the canopy
h	surface-near relative air humidity
T; T_{MAX}; T_{MIN}	surface-near air temperature; monthly maximal and minimal daily temperature
T_{NEW}; T_{OLD}; γ	air temperature after and before correction, γ correction factor (see section 3.1.1)
T_{LEAF}	leaf temperature
R_{ECO}	ecosystem respiration = autotrophic + heterotrophic respiration
A	assimilation rate
R_{LEAF}	leaf respiration equals 15% of A
NPP	net primary productivity (CO_2)
GPP	gross primary productivity (CO_2)
GPP_{O2}	O_2 flux corresponding to the gross primary productivity; GPP_{O2} is balanced by R_{ECO}
R_{PHOTO}; PHO_{O2}	O_2 consuming flux during photorespiration exactly balanced by a production rate of O_2, PHO_{O2}
R_{MEHLER}; P_{MEHLER}	O_2 flux corresponding to other O_2 reactions during photosynthesis, estimated as 10% of R_{ECO} (D. Yakir, personal communication, 2001); the flux is balanced by a production rate P_{MEHLER}
Vo, Vc, $\zeta = $ Vo/Vo	oxygenation and carboxylation rate in moles of RuBP (ribulose bisphospate) and their relation as defined by *Farquhar et al.* [1980]
Γ^*	CO_2 compensation point calculated as by *Lloyd and Farquhar* [1994]
Ci	inner cellular CO_2 concentration calculated as by *Lloyd and Farquhar* [1994]
ε_{ECO}	fractionation at ecosystem respiration; = 95% × 19.2‰ (cytochrome pathway) + 5% × 30.8% (alternative pathway) = 20.35‰ (J. Berry, personal communication, 2002) [*Robinson et al.*, 1992]
ε_{PHOTO}	fractionation at photorespiration = 21.7‰ [*Guy et al.*, 1993]
ε_{MEHLER}	fractionation during the Mehler reaction = 15.3‰ [*Guy et al.*, 1993]
ε_{EQUIL}	= 9.35‰ at 25°C, equilibrium fractionation during the phase transition between water vapor and liquid water [*Farquhar et al.*, 1989]
ε_{KIN}	= −26.35‰ kinetic fractionation during diffusion of water vapor from inside the leaf to the air [*Farquhar et al.*, 1989]
O_{2DISS}	dissolved molecular oxygen in the ocean
$\delta^{18}O_{DISS}$	$^{18}O/^{16}O$-relation of O_{2DISS} in δ-notation
Σ	ocean salinity
S_{GLOBAL}	global mean ocean salinity
PP	marine primary productivity
Rem	organic material remineralized within the euphotic layer
f-ratio, f = (PP-Rem)/PP	f-ratio of exported organic material to primary productivity as defined by *Eppley and Peterson* [1979]

0.05 and 0.14. This corresponds to a reduction of the effective relative humidity near the leaves of up to 15% compared to the monthly mean average computed by the AGCMs.

3.1.2. Oxygen Fluxes of the Terrestrial Biosphere

[14] We infer the biome distribution and the terrestrial O_2 fluxes of photosynthesis and total respiration from two global TBMs, SLAVE [*Friedlingstein et al.*, 1992, 1995a, 1995b] and SILVAN [*Kaduk*, 1996; *Kaduk and Heimann*, 1996]. The biome distribution is predicted by a classification scheme being part of the SLAVE model and by the BIOME1 model for SILVAN. The respiratory uptake of O_2 discriminates against the heavier isotopomer $^{18}O^{16}O$ in a different manner for (1) ecosystem respiration, R_{ECO}, i.e., the sum of autotrophic and heterotrophic respiration, (cytochrome and alternative pathway), (2) photorespiration, R_{PHOTO}, and (3) several other O_2 consuming reactions such as the Mehler reaction or chlororespiration, which we subsume under the Mehler reaction in a generic manner, R_{MEHLER}. All three quantities are estimated separately. The

terrestrial Dole effect Δ_T is then calculated on the grid of the corresponding TBM on a monthly basis. This yields

$$\Delta_T = \left(\sum_{i,M}^{N,\text{Month}} P_T^{i,M} * \delta_{LEAF}^{i,M} + \varepsilon_{ECO} * R_{ECO} + \varepsilon_{PHOTO} * R_{PHOTO} + \varepsilon_{MEHLER} * R_{MEHLER} \right) / P_T - \delta^{18}O_{OW}. \quad (3)$$

The derivation of this formula is very similar to the computation of the steady state budget of other isotopic tracers (for example, for the ^{18}O in CO_2 of *Ciais et al.* [1997a]).

[15] Assuming that the biosphere model is in a steady state, these respiratory fluxes are exactly balanced over a year by corresponding O_2 fluxes released during photosynthesis. Each of the oxygen consumption fluxes is affected by a specific, spatially and temporally constant fractionation, ε_{ECO}, ε_{PHOTO}, and ε_{MEHLER}. Here ε_{ECO} is estimated as a weighted mean of fractionation during the cytochrome and

the alternative pathway, and ε_{MEHLER} is chosen as the measured fractionation of the Mehler reaction (see Table 2). On top of that, O_2 in water is enriched by about 0.7 ‰ with respect to air [*Benson and Krause*, 1984] so that the overall respiratory fractionation is reduced by this amount.

[16] The terrestrial O_2 production, P_T, is isotopically tagged by the leaf water as it is produced during water splitting reactions during photosynthetic. For the sake of clarity, we distinguish the oxygen fluxes relevant in this study from the corresponding carbon fluxes by an index, O_2, attached to the usual terms, that is GPP_{O2} (PHO_{O2}) for the oxygen released during photosynthesis (photorespiration) and corresponding to the carbon Gross Primary Production, GPP. With this notation, we thus have $P_T = GPP_{O2} + PHO_{O2} + P_{Mehler}$. Both TBMs are using quite different methods for estimating P_T, which are explained in detail as follows.

[17] 1. The SLAVE model uses the biome classification scheme following *Olson et al.* [1985] and aggregates the original 52 biomes of the Olson scheme to 9 biomes. The biomes grassland and savannah are recombined into C3 and C4 type grasses according to a CO_2 dependent threshold temperature criteria [*Haxeltine and Prentice*, 1996]. This separation is of particular importance because C4 grasses avoid the energetic disadvantages of photorespiration by a mechanism that concentrates CO_2 in specialized plant tissue. The SLAVE model first infers the net primary production (NPP) following a light use efficiency formulation [*Field et al.*, 1995]. The assimilation rate, A, is calculated by means of a simple linear relationship from NPP using a biome dependent factor, φ, which describes the proportion of A lost as plant respiration [*Lloyd and Farquhar*, 1994]: $A = NPP/(1 - \varphi)$. Subsequently, GPP is calculated assuming a fixed percentage of 15% of leaf respiration, R_{LEAF}: $GPP = A + R_{LEAF} = 1.15 \times A$. The percentage of R_{LEAF} which denotes mitochondrial CO_2 release through the stomata is a very stable estimate obtained from mechanistic biosphere models [*Farquhar et al.*, 1980]. In the next step, photorespiration is estimated as a fraction of the calculated GPP. According to *Farquhar et al.* [1980] the parameter ξ describes the molar relation of oxygenation, Vo, to carboxylation, Vc, of the primary carbon acceptor molecule ribulose bisphosphate, RuBP, i.e., $\xi = Vo/Vc$. From the stoichiometry of the photorespirative reaction [*von Caemmerer*, 2000], one knows that for each oxygenation the plant loses half a mole of CO_2. Therefore, in terms of CO_2 fluxes, the gross primary production reads as

$$GPP = \text{Carboxylation} - 1/2 \times \text{Oxygenation}$$
$$= (1. - 0.5 \times \xi) \times \text{Vc}.$$

In terms of O_2 we have

$$GPPO_2 = \text{Carboxylation} + \text{Oxygenation} = (1. + \xi) \times \text{Vc}.$$

This means that for each mole of photorespired CO_2 (0.5ξ). three moles of O_2 (1.5ξ) are involved: 2 moles for the oxidation of RuBP and 1 mole for the oxidation of Phosphoglycolate. The CO_2 compensation point, Γ^*, is defined as the CO_2 concentration with as much carboxyla-

tion as oxygenation: $\xi = 2\,\Gamma^*/Ci$. In summary, the relation of GPP to GPP_{O2} then reads as

$$GPP_{O2}/GPP = (1. + \xi)/(1. - 0.5 \times \xi) = (Ci + 2\Gamma^*)/(Ci - \Gamma^*).$$

Following *Lloyd and Farquhar* [1994], we estimate Γ^* simply as $\Gamma^* = 2 \times T_{New}$ where T_{New} denotes the modified air temperature (see Table 2). Ci is calculated as a function of biome dependent parameters [*Lloyd and Farquhar*, 1994]. However, it is possible that an additional half a mole of O_2 is used within photorespiration for the regeneration of products of the glycine cycle (J. Berry, personal communication, 2002). Additional O_2 consumptions like the Mehler reaction are estimated for both TBMs as 10% of GPP (D. Yakir, personal communication, 2001).

[18] 2. The SILVAN model, the second biosphere model used in this study, is a mechanistic model based on our knowledge of the biochemistry of plants. It calculates photosynthetic fluxes (CO_2, O_2) depending on monthly precipitation, temperature, and cloud coverage as external climate forcing (see Figure 2). Photorespiration is deduced from the calculated GPP in the same manner as for the SLAVE model. Most of the physiological parameters of the model depend on the corresponding biome type determined by the BIOME1 classification scheme [*Prentice et al.*, 1992]. Again, the original 18 biomes of SILVAN have been aggregated here to the same 9 biome types mentioned above. The biosphere ecosystem respiration in both models is assumed to be in equilibrium with climate and therefore balances annual photosynthesis both in terms of CO_2 and O_2 fluxes for every grid cell. The TBMs are run with different observed climatologies from *Shea* [1986] and *Cramer and Leemans* [1991], respectively. Basic construction and principles employed in both TBMs are fundamentally different. SLAVE is a heuristic model calculating the CO_2 fluxes based on empirical relationships. Conversely, SILVAN uses mechanistic formulations for inferring photosynthesis. We therefore believe that the two TBMs allow us to bracket the range of possible solutions for the DE through different patterns and strengths of the modeled O_2 fluxes.

3.2. Ocean

[19] In the early days of oceanic isotopic tracer studies the isotopic composition of dissolved oxygen has been discussed as a particularly interesting tracer of both marine productivity and oceanic circulation. It is the only tracer directly linked to the oceanic carbon cycle that reacts nonlinearly on production and remineralization, i.e., not according to the fixed proportions of the Redfield ratio. Therefore it was suggested to use this isotope signal to separate biological and transport processes in the deep ocean [*Bender*, 1990; *Kroopnick*, 1987].

[20] In our approach to model the marine DE, we use the global ocean carbon cycle model HAMOCC3.1 [*Maier-Reimer*, 1993; *Six and Maier-Reimer*, 1996]. It transports various biochemical tracers in an offline mode using monthly transport fluxes of a 3D-ocean general circulation model [*Maier-Reimer et al.*, 1993]. HAMOCC3.1 includes a plankton sub-model to estimate the net marine primary productiv-

ity and oxygen consumption by heterotrophic respiration during remineralization. This plankton sub-model achieves a good representation of the fast biological overturning in the euphotic zone. It consists of five components: phytoplankton, zooplankton, detritus, dissolved organic carbon, and nutrients (PO_4). Inclusion of the plankton sub-model clearly improved the capacity of the model to simulate seasonal variations of pCO_2 and the corresponding O_2 fluxes. Radiative forcing at the ocean surface influencing the biological activity in the euphotic zone is taken from the ECHAM3 control simulation. We run HAMOCC3.1 in a reduced two and a half dimensional geometry, which allows us long-term integrations. The zonal resolution was changed to one Atlantic and one Pacific grid box by keeping a meridional resolution of 5 degrees and 11 layers in the vertical. An additional meridional mixing is parameterized to account for the zonal inhomogeneity of the 3D fluxes.

[21] Although the geometrical simplification of a two and a half dimensional ocean circulation does decrease the sensitivity of the model to non-zonal forcing mechanisms such as wind driven regional upwelling, the zonal version of the model simulates reasonably well the distribution of several oceanic tracers such as bomb C_{14} and PO_4^* [*Weber*, 1996].

[22] The HAMOCC3.1 is brought into equilibrium with an overlying one-layer diffusive atmosphere. The quantity Δ_O corresponds to the asymptotic $\delta^{18}O_{ATM}$ which the ocean model attains in its biogeochemical steady state after some 10,000 years integration time. Both dissolved $^{16}O_2$ and $^{18}O^{16}O$ are treated as independent geochemical tracers. A small temperature dependent fractionation of 0.7‰ takes place when atmospheric oxygen is dissolved into the sea [*Benson and Krause*, 1984]. The photosynthetic ocean source of O_2 matches isotopically the composition of surface waters $\delta^{18}O_{EUPH}$, which is itself regressed from the salinity field [*Broecker*, 1986; *Duplessy et al.*, 1991] according to $\delta^{18}O_{OW} = 0.5 \times (S - S_{GLOBAL})$. S denotes local salinity and S_{GLOBAL} denotes the global average of S. We will discuss the robustness of this assumption later.

[23] The respiratory sink of dissolved O_2 is represented in the model with a constant fractionation of 20‰ [*Kiddon et al.*, 1993]. However, these authors pointed out the large uncertainties of this value. Even when restricting the analysis on the dominant marine respiring organisms (bacteria, microalgae, and zooplankton), they estimated an uncertainty of ±3‰ to the mean 20‰. This value used in the study here is probably rather on the lower end of today's estimates for marine respiration. In a study restricted to the subarctic Pacific, for example, *Quay et al.* [1993] calculated a mean fractionation during respiration of 22‰ ± 6‰.

4. Results

4.1. Terrestrial Environment

[24] The isotopic composition of leaf water deduced from the two AGCMs is shown in Figure 3. In both graphs, $\delta^{18}O_{LEAF}$ has been tuned to match the observed DE. Both models show a similar global distribution of $\delta^{18}O_{LEAF}$, which is mainly due to the similarity of their respective background-water isotope fields (precipitation and groundwater). For

example, they feature a strong latitudinal gradient in the Northern Hemisphere closely following the "temperature effect" of stable isotopes in precipitation [*Dansgaard*, 1964]. Over vegetated areas, lowest values are simulated over north-eastern Siberia $\delta^{18}O_{LEAF} \sim -16‰$) which results from very depleted surface waters on one hand and a relative humidity close to saturation on the other hand (see equation (2)). Very high values are reached in the subtropical dry belts of both hemispheres where productivity is low, however. The impact of these high values on the global DE remains therefore rather small. Over the tropical rain forests and seasonal forests of South America and Central Africa the models estimate a water isotopic depletion being more negative (between 5 and 10‰) compared to the adjacent savannah and semi-desert dominated regions. The only larger difference between both models appears in southeast Asia where the GISS model simulates nearly all year long humid conditions with a more depleted composition of leaf water than ECHAM, which is characterized by a marked seasonality of both humidity and the water isotopes caused by a too strong monsoon circulation.

[25] The striking overall correspondence of both models is also demonstrated in Figure 4a showing the zonal means of $\delta^{18}O_{LEAF}$ of the three analyzed model combinations. The maximal deviation between the zonal means amounts to 5–10‰ and is strongest in the subtropics where it is less relevant for the global DE. The differences between both TBMs (SLAVE/SILVAN) are apparently more significant. The global productivity of both models is quite similar (17.9 Pmol O_2 for SLAVE and 15.5 Pmol O_2 for SILVAN). However, the zonal distribution of the O_2 fluxes estimated by the SLAVE model (Figure 4b) shows a tropical production about twice as high as in northern midlatitudes. In contrast, the fluxes inferred by the SILVAN model are only about 40% stronger in the tropics than in midlatitudes. This has some consequences for the final latitudinal contribution to the DE (Figure 4c). The ECHAM/SILVAN DE gives more weight to middle northern and southern latitudes relative to the tropics than the two SLAVE model combinations. A validation of these model results can only be achieved by future high precision measurements that possibly will allow estimating the latitudinal structure of the ^{18}O sources and sinks (for first results, see *Seibt* [2003]).

[26] As explained previously, we have recombined the terrestrial oxygen fluxes (PMol) and the contribution to the DE (‰) into nine different biome types (Figures 5a and 5b, respectively). The strongest difference between the heuristic model (SLAVE) and the mechanistic model (SILVAN) is the different contribution of evergreen forest relative to C4 grasses and tropical seasonal forest. The SILVAN model computes for all three biomes a nearly equal contribution to the global balance of O_2 and the DE. The SLAVE model, however, estimates that the tropical evergreen forests contributes about 40% stronger to both budgets than C4 grasses or seasonal forest. This difference is principally due to the differences in both TBM's biome classification scheme. It reflects largely the considerably higher fraction of grasslands in the biome distribution used in SILVAN which was predicted by the BIOME model compared to the SLAVE model. In both models, the biome type "grasslands" is then
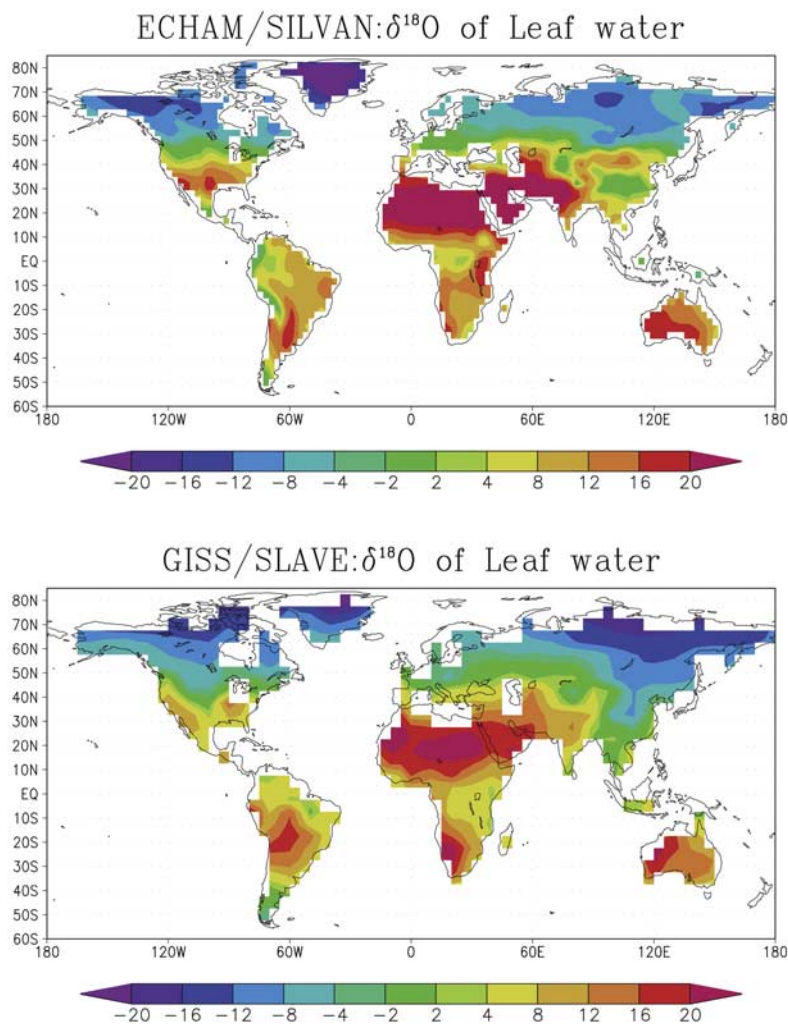
Figure 3. The $\delta^{18}O$ value of leaf water deduced from the *Craig and Gordon* [1965] formula (see text for details) using water isotope fields which were simulated by the (top) ECHAM and (bottom) GISS model. The global integral is $\delta^{18}O_{Leaf} = 6.8‰$ for the ECHAM model and $\delta^{18}_{Leaf} = 6.3‰$ for the GISS model.

separated into C3 and C4 grasses according to a temperature criterion.

4.2. Marine Environment

[27] The model calculates an isotopic composition of the atmosphere in the ocean-only simulation and thus a marine Dole effect Δ_O of 16.97‰. The simulated oceanic meridional distribution of $\delta^{18}O_{DISS}$ is shown in Figure 6a for both basins, Atlantic and Indo-Pacific, together with the corresponding O_2 distribution Figure 6b. The shown $\delta^{18}O_{DISS}$ values must be interpreted relative to the atmospheric equilibrium value Δ_O. As expected both tracers, $\delta^{18}O_{DISS}$ and O_{2DISS}, are closely linked to each other. Zones of strong oxygen consumption are characterized by a correspondingly enriched $\delta^{18}O_{DISS}$ signal due to the fractionation during remineralization. A particularly strong signal can be seen in the tropical ocean just below the thermocline between 100 and 1000 m depth. Here the dissolved oxygen is enriched by about 14–16‰ in the

Atlantic and by 45‰ in the Pacific. In the same regions the corresponding O_{2DISS} concentrations are lower by about 120 μmol/L in the Atlantic and 2 μmol/L in the Pacific. Whereas in the Atlantic basin the model results are quite realistic, both oxygen utilization and $\delta^{18}O_{DISS}$ values are not in agreement (both too large) with the observations in the Indo-Pacific [*Kroopnick*, 1987]. This disagreement is caused by the phenomenon of nutrient trapping which exists to some extent in nature too but is often largely overestimated in ocean carbon cycle models [*Maier-Reimer*, 1993; *Najjar*, 1990; *Six and Maier-Reimer*, 1996]. It reflects a positive feedback mechanism between intense production induced by upwelling nutrient-rich abyssal waters and remineralization of organic matter in the tropical divergence zone. It is not clear if this chronic problem of ocean models is a result of an oversimplification of the ocean's biogeochemistry by neglecting longer-living carbon pools [*Six and Maier-Reimer*, 1996] or caused by problems in the circulation field [*Aumont et al.*, 1999]. As in a previous study with
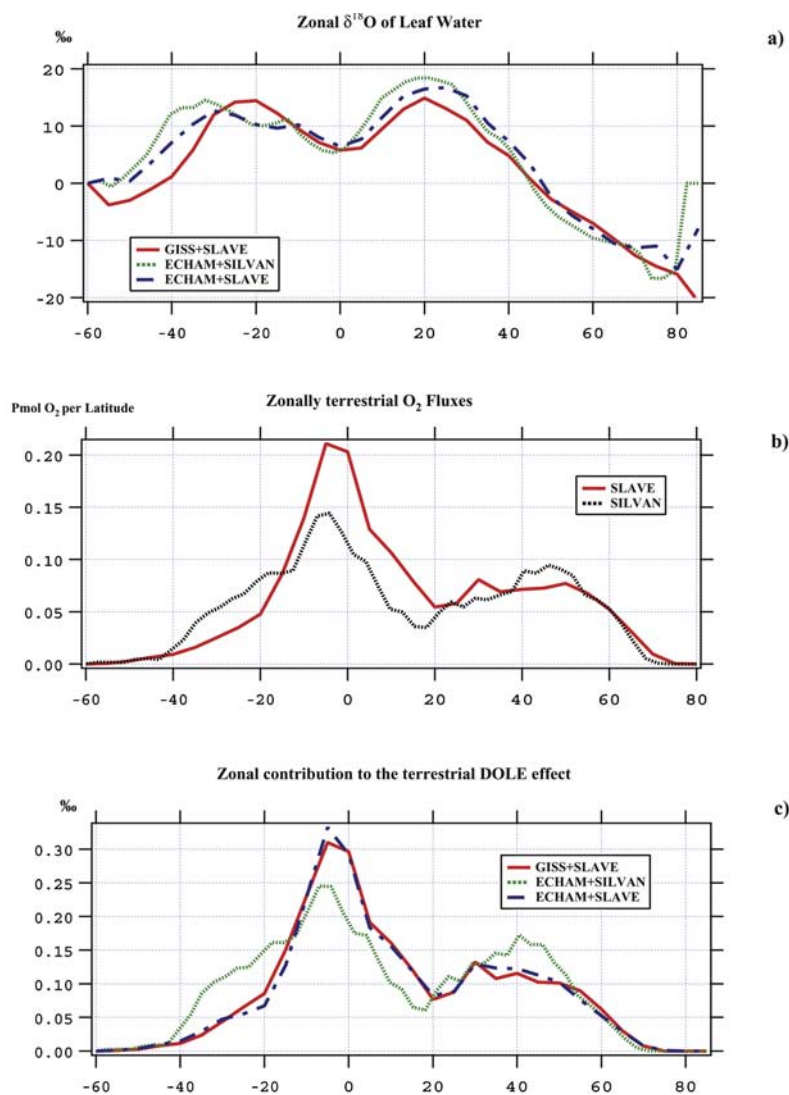
Figure 4. Zonal means of (a) $\delta^{18}O_{Leaf}$ derived from the three model combinations, (b) of terrestrial O_2 fluxes calculated by the two TBMs, and (c) of the terrestrial Dole effect Δ_T (see equation (3) in the text; units are ‰ per degree latitude; the latitudinal integral of the curves in Figure 4c gives the corresponding global terrestrial DE) again from the three model combinations.

the three-dimensional HAMOCC3, the model results generally agree well with the comparably sparse observations from the GEOSECS program [*Kroopnick*, 1987]. The model, however, systematically tends to overestimate the isotopic oxygen enrichment as already noted by *Maier-Reimer* [1993]. Simulated $\delta^{18}O_{DISS}$ values of dissolved oxygen were larger than 35‰ corresponding approximately to an oxygen concentration lower than 30% relative to the saturation value. A detailed comparison between modeled and observed $\delta^{18}O_{DISS}$ concentration will become an interesting model application of the oxygen isotopes in the future but will not be further discussed here.

[28] In order to evaluate the simulated Δ_O, we have to determine the main controls on Δ_O. In particular we have to find out how strongly Δ_O is affected by the potentially overestimated nutrient trapping in the Pacific. The latter is certainly not a serious problem since the volume of the

ocean concerned is quite small. Moreover, the low oxygen concentrations in the equatorial divergence zone guarantee that the overall ^{18}O budget of the ocean is hardly affected by the locally overestimated $\delta^{18}O_{DISS}$ values. In contrast, the simulated $\delta^{18}O_{DISS}$ values in the deep ocean are nicely corroborated by observations. In the Atlantic below 2000 m, the observed $\delta^{18}O_{DISS}$ enrichment [*Kroopnick*, 1987] relative to the atmospheric value of 23.5‰ is in the range between 1 and 6‰ (the model simulates 2–4‰). In the Pacific, which is characterized by considerably older water masses, $\delta^{18}O_{DISS}$ vary between 4 and 8‰ (model: 4–12‰).

[29] However, the ocean's overall DE is primarily determined by processes in the euphotic layer where most of the remineralization of organic material occurs. In fact, the more remineralization of organic material occurs in the euphotic layer, the closer the $\delta^{18}O_{DISS}$ is to the respiratory
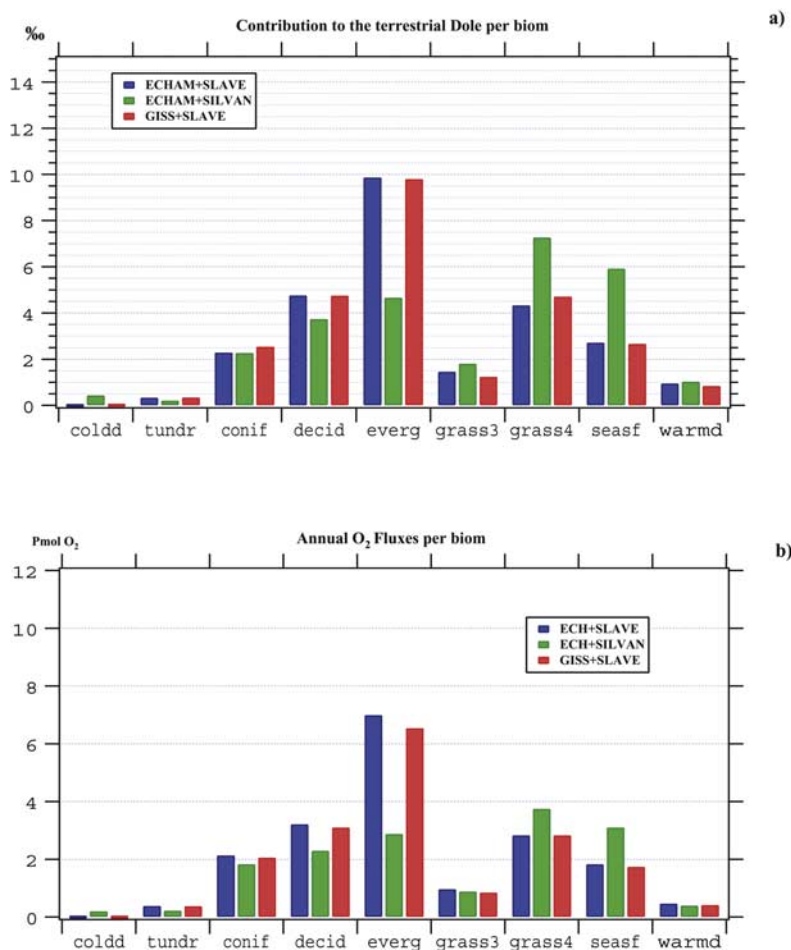
Figure 5. Contribution to the (a) terrestrial DE (units are ‰ per biome) and (b) O_2 fluxes for different biomes. The biome types shown in the graph (cold desert, tundra, coniferous forest, deciduous forest, evergreen forest, C3 and C4 grasses, seasonal forest, warm desert) are aggregated from the original biome types used in the TBMs for a better presentation (see the text for the exact association). The sum of all biomes both for the terrestrial DE (Figure 5a) and for the O_2 fluxes (Figure 5b) amounts to the global values given in Table 1.

limit of 20‰. Conversely, the more oxygen is produced in excess to respiration in the upper 100 m, the closer $\delta^{18}O_{DISS}$ is to $\delta^{18}O_{EUPH}$ (i.e., nearly 0‰ for today's conditions).

[30] The relation between net primary production and remineralization within the euphotic layer is usually expressed by the f-ratio, f = (PP-Rem)/PP with PP as primary productivity and Rem as the part of PP which is already remineralized in the euphotic zone. HAMOCC3.1 simulates a global f-ratio of 0.2. This is in agreement with *Eppley and Peterson* [1979], who estimated a global value of f = 0.1 − 0.2. However, we calculate a net primary productivity of 62.9 GtC/yr which is well above all estimates based on observations such as the one by *Eppley and Peterson* [1979], who scaled up local observations (PP of about 19.1–23.7 GtC/yr) or by *Antoine et al.* [1996], who obtained a range of 36.5–45.6 GtC/yr on the basis of satellite observations. Still, these estimates are affected by large uncertainties, and therefore we consider our simulated value in accordance with our present knowledge of marine

productivity. The simulated F ratio varies slightly both regionally (f = 0.19–0.21) and seasonally (f = 0.17–0.23).

[31] Our hypothesis that the relation between PP and Rem, thus the f-ratio, controls the oceanic Dole effect was confirmed by a sensitivity experiment. We reduced artificially the export of organic material out of the euphotic layer and thus made more organic material available for respiration. This changing in the parameterization diminished the f-ratio to 0.1 and therefore gave more weight to the respiration fractionation of 20‰. The oceanic DE rises as expected in this experiment to 18.27‰.

[32] In order to better assess the uncertainties in our ocean model, we now focus on two potentially important model assumptions. First, we assume that there is no planktonic autorespiration, a process that delivers energy for maintaining the biochemical reactions in terrestrial plants. Though it is sensible to assume that planktonic autorespiration is generally smaller than its analogue on land, no quantitative estimates of this process exist. In a sensitivity experiment,
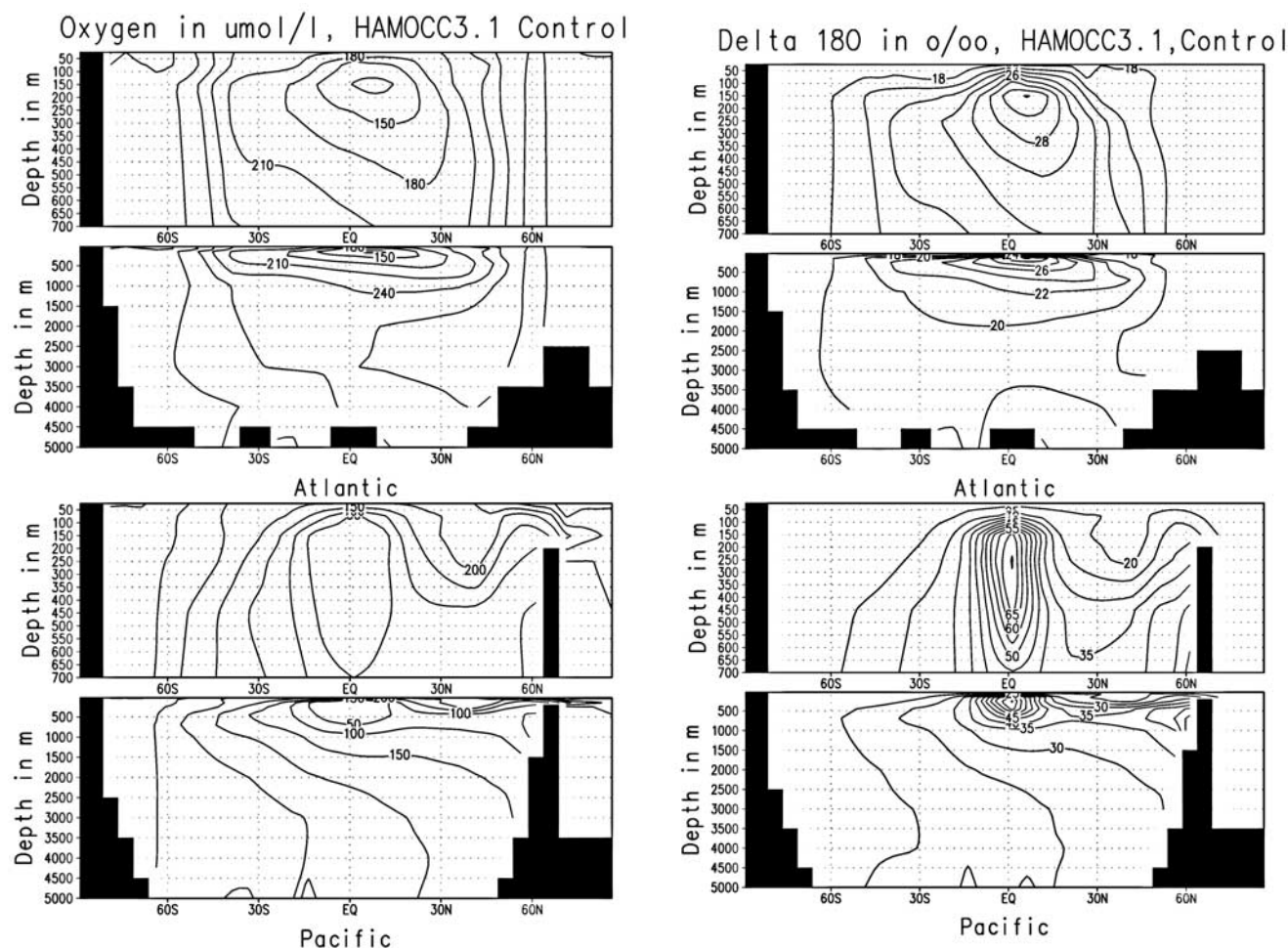
Figure 6. (left) Dissolved oxygen concentration in μmol/l as simulated for the two basins (Atlantic, top panel, and Indo-Pacific, bottom panel) of the two-dimensional HAMOCC3.1 ocean carbon cycle model. (right) The $\delta^{18}O$ of dissolved oxygen as simulated for the two basins (Atlantic, top panel, and Indo-Pacific, lower panel) of the two-dimensional version of the HAMOCC3.1 ocean carbon cycle model. All values presented are relative to the atmospheric $\delta^{18}O$ value of 16.93‰, i.e., Δ_O.

we doubled the oceanic O_2 flux by a part which is directly respired in the euphotic zone (hence the autorespiration would correspond to a fraction of 50% of the total respiration). This changed the global F value from 0.20 to 0.10 and enhanced the Dole effect by about 2‰.

[33] Second, our model assumes that $\delta^{18}O_{EUPH}$ follows salinity in the entire ocean by a linear relationship of 0.5‰/psu. There are, indeed, considerable regional deviations from this global relationship. In the tropics, for example, the ^{18}O-salinity relation is typically more flat, i.e., on the order of 0.3‰/psu, whereas, in polar regions, it is steeper mainly due to isotopic effects induced during sea ice formation. However, a sensitivity study in which we prescribed the isotopic composition of the entire ocean to 0‰ demonstrated only a weak response of the DE (<0.1‰) to the detailed geographical distribution of the surface isotope signal $\delta^{18}O_{EUPH}$. This holds principally since the production weighted mean isotopic composition of the ocean's surface waters is in both cases approxi-

mately 0‰. Strong marine productivity in high latitudes with isotopically more depleted surface waters are nearly balanced by an equally strong production in the upwelling zones of low latitudes with more enriched surface waters.

5. Discussion and Perspectives

[34] In our model construction, we match the observed DE by tuning the least known quantity, i.e., the isotopic composition of leaf water, $\delta^{18}O_{LEAF}$. Even without any tuning, our process-based results (between 22.4‰ and 23.3‰) are already close to the observations. Nevertheless, this cannot be taken as an argument against possible additional fractionation effects such as by diffusion of oxygen molecules in soils [*Angert et al.*, 2001], which have not been taken into account in this study.

[35] A regional comparison between our estimates of $\delta^{18}O_{LEAF}$ and the rare observations is unfortunately not feasible. Differences between various plant species within

the same biome type are quite large [*Wang and Yakir*, 1995] and make it necessary to compute $\delta^{18}O_{LEAF}$ for each biome from each of the composing plant species.

[36] The relatively good process-based prediction of the DE is mainly due to a larger global $\delta^{18}O_{LEAF}$ estimated by both AGCMs employed here, ECHAM3 and GISS model, than assumed in previous studies. However, as already pointed out by *Keeling* [1995], such a large enrichment in leaf water is not in agreement with our current understanding of the global budget of ^{18}O in CO_2. Basically the same processes but with an opposite sign affect the global isotopic cycle of $C^{18}O^{16}O$. When plants consume CO_2 during photosynthesis they produce O_2 and vice versa during respiration. With the best estimates for the various CO_2 fluxes *Farquhar et al.* [1993] could balance the $C^{18}O^{16}O$ budget by assuming a global leaf water enrichment of 4.4‰ compared to the value of 6.1–6.8‰ as deduced here. However, there are some significant differences between the geochemical cycles of O_2 and CO_2. First, in the presence of the catalyzing enzyme carbonic anhydrase, ubiquitous in plant tissue, carbon dioxide equilibrates isotopically in a very short time with the surrounding water. Since about two thirds of the CO_2 entering the stomata is directly rediffused, a large part of the isotopically affected CO_2 does not proceed to the chloroplasts where the uptake of CO_2 takes place and finally the O_2 molecules are emitted by the photosynthetic reaction. The possible isotopic differences between leaf water at the surface of the stomata, controlling the isotopic composition of CO_2, and inner cellular chloroplast water, relevant for the isotopic composition of O_2, does however enlarge even the problem of constructing a common budget of $\delta^{18}O$ of CO_2 and O_2. The water directly exposed to the evaporation into the stomata is isotopically more enriched than the chloroplast water. The spatial separation of CO_2 and O_2 equilibration and the isotopic difference of water at both locations in plant tissue might help to reconcile both budgets. A further possibility for a higher $\delta^{18}O_{LEAF}$ tagging the produced O_2 compared to the CO_2 was discussed by *Gillon and Yakir* [2001]. The effective activity of the carbonic anhydrase shows strong plant type dependent variability. In particular, in C4 plants, the activity of the carbonic anhydrase enzyme is nearly 60% lower than in equivalent C3 plants. On the basis of in situ measurements, the authors estimated an effective global equilibration for the CO_2 of only 80%. Second, CO_2 produced by heterotrophic respiration diffuses through the soil column and equilibrates all the time with the surrounding soil water. According to the estimates of *Miller et al.* [1999] and *Riley et al.* [2002], the emitted CO_2 is in equilibrium with soil water below 15 cm. A lower isotopic composition of soil water than calculated by *Ciais et al.* [1997a] and *Farquhar et al.* [1993], and an increased isotopic composition of leaf water could bring both isotope budgets into agreement (M. Bender, cited according to *Keeling* [1995]). A mechanistic description of such processes in soils, however, involves a detailed description of evaporation from soils affecting the $\delta^{18}O$ gradient of water in the soil and of water uptake in various depths by plant roots controlling the isotopic composition of leaf water. Such an isotope soil hydrology is neither built into the GISS

nor into the ECHAM model, which both describe soil processes by a simple one-layer bucket model.

[37] Comparing our estimates of global terrestrial and marine O_2 fluxes and corresponding DEs with the estimates of *Bender et al.* [1994b] reveals some interesting features. Our model calculation estimates the annual production of O_2 in both environments smaller than in Bender et al.'s approach (P_O is about 40% and P_T about 15% smaller than in the budget of *Bender et al.* [1994b]) resulting in a relation between the marine and the terrestrial productivity of about one half relative to about two thirds in the work of *Bender et al.* [1994b]. Consequently, there is a slightly different contribution to the overall DE by both biospheres in the two approaches.

[38] The lower production rates of O_2 in our calculation results in an atmospheric O_2 turnover time of about 1500 years in contrast to the 1200 years inferred from *Bender et al.* [1994b]. Given that these O_2 fluxes are most probably even lower during glacial conditions, this has some consequences when interpreting the $\delta^{18}O_{ATM}$ signal of ice cores and its leads and lags relative to the other information deduced from the ice such as CO_2 or local temperature [*Broecker and Henderson*, 1998].

[39] Furthermore, our oceanic Dole effect is about 2‰ lower as in the work of *Bender et al.* [1994b]. This result certainly needs further investigation, for example with different ocean biosphere models like our terrestrial approach with different TBMs. In situ measurements performed at all U.S. JGOFS stations indicate, for example, a considerably lower relation between productivity inferred from ^{14}C incubated water samples and O_2 production than the one used in our model. The additional O_2 fluxes might be related to autorespirative processes such as photorespiration or the Mehler reaction in the ocean biosphere (M. Bender, personal communication, 2002). The sensitivity experiment (50% larger O_2 fluxes and hence lower f-ratio) discussed above captures such a scenario and resulted in a 2‰ larger oceanic DE.

[40] Furthermore, it is planned to address the problem of the diverging isotope budgets of CO_2 and O_2 by using a mechanistic TBM built into the ECHAM model. This will also allow us to calculate synchronously over the daily cycle the isotopic composition of leaf and soil water together with the biospheric fluxes of O_2 and CO_2 [*Cuntz et al.*, 2003a, 2003b].

[41] The difference between Δ_T and Δ_O estimated from our standard experiment becomes as large as 10.7‰ instead of 4‰ in M. Bender's best guess (see Table 1). The difference has to be weighted by the relation between terrestrial and marine productivity. Even slight changes in the relation of P_O and P_T in the quaternary would then have a strong impact on the DE. The astonishing stability of the DE observed over the last two glacial interglacial cycles (±0.5‰) argues for strong natural compensation effects between the different processes affecting the DE, at least on timescales beyond a few thousand years. Such compensating effects, however, might not operate over the next few hundred years when substantial anthropogenically induced changes may affect the Earth's climate and the terrestrial and marine biosphere. Process-based models of the Earth's

Dole effect such as the one described here are needed to explore the factors responsible for the apparent stability of the Dole effect in the past, and to estimate possible shifts of the Dole effect in the future.

References

Angert, A., B. Luz, and D. Yakir (2001), Fractionation of oxygen isotopes by respiration and diffusion and its implications for the isotopic composition of atmospheric O$_2$, *Global Biogeochem. Cycles*, *15*(4), 871–880.

Antoine, D., J.-M. André, and A. Morel (1996), Oceanic primary production: 2. Estimation at global scale from satellite (coastal zone color scanner) chlorophyll, *Global Biogeochem. Cycles*, *10*(1), 57–69.

Aumont, O., J. C. Orr, P. Monfray, G. Madec, and E. Maier-Reimer (1999), Nutrient trapping in the equatorial Pacific: The ocean circulation circulation solution, *Global Biogeochem. Cycles*, *13*(2), 351–369.

Bariac, T., J. Gonzalez-Dunia, N. Katerji, O. Béthenod, J. M. Bertolini, and A. Mariotti (1994), Variabilité spatiale de la composition isotopique de l'eau (18O,2H) dans le continuum solplante-atmosphère: Approche en condition naturelles, *Chem. Geol.*, *115*, 317–333.

Bender, M. L. (1990), The δ^{18}O of dissolved O$_2$ in seawater: A unique tracer of circulation and respiration in the deep sea, *J. Geophys. Res.*, *95*(C12), 22,243–22,252.

Bender, M., T. Sowers, M.-L. Dickson, J. Orchado, P. Grootes, P. A. Mayewski, and D. A. Meese (1994a), Climate correlations between Greenland and Antarctica during the past 100,000 years, *Nature*, *372*, 663–666.

Bender, M., T. Sowers, and L. Labeyrie (1994b), The Dole effect and its variations during the last 130,000 years as measured in the Vostok ice core, *Global Biogeochem. Cycles*, *8*(3), 363–376.

Benson, B., and D. Krause (1984), The concentration and isotopic fractionation of oxygen dissolved in fresh water and seawater in equilibrium with the atmosphere, *Limnol. Oceanogr.*, *318*, 349–352.

Broecker, W. S. (1986), Oxygen isotope constraints on surface ocean temperatures, *Quat. Res.*, *26*, 121–134.

Broecker, W. S., and G. M. Henderson (1998), The sequence of events at termination II and their implications for the cause of glacial-interglacial CO$_2$ changes, *Paleoceanography*, *13*(4), 352–364.

Ciais, P., P. P. Tans, M. Trolier, J. W. White, and R. Francey (1995), A large Northern Hemisphere terrestrial CO$_2$ sink indicated by the ^{13}C/^{12}C ratio of atmospheric CO$_2$, *Science*, *269*, 1098–1102.

Ciais, P., S. A. Denning, P. P. Tans, J. A. Berry, D. A. Randall, G. J. Collatz, P. J. Sellers, J. W. C. White, P. Monfray, and M. Heimann (1997a), A three-dimensional synthesis study of δ^{18}O in atmospheric CO$_2$: 1. Surface fluxes, *J. Geophys. Res.*, *102*(D5), 5857–5872.

Ciais, P., et al. (1997b), A three-dimensional synthesis study of δ^{18}O in atmospheric CO$_2$: 2. Simulations with the TM2 transport model, *J. Geophys. Res.*, *102*(D5), 5873–5883.

Craig, H. (1961), Standard for reporting concentrations of deuterium and oxygen-18 in natural water, *Science*, *133*, 1833–1834.

Craig, H., and L. I. Gordon (1965), Deuterium and oxygen-18 variations in the ocean and the marine atmosphere, in *Stable Isotopes in Oceanographic Studies and Paleotemperatures*, edited by E. Tongiorgi, Cons. Naz. delle Ric., Lab. di Geol. Nucl., Pisa, Italy.

Cramer, W. P., and P. Leemans (1991), The IIASA database for mean monthly values of temperature, precipitation, and cloudiness on a global terrestrial grid, Int. Inst. for Appl. Syst. Anal., Laxenburg, Austria.

Cuntz, M., P. Ciais, G. Hoffmann, and W. Knorr (2003a), A comprehensive global three-dimensional model of δ^{18}O in atmospheric CO$_2$: 1. Validation of surface processes, *J. Geophys. Res.*, *108*(D17), 4527, doi:10.1029/2002JD003153.

Cuntz, M., P. Ciais, G. Hoffmann, C. E. Allison, R. J. Francey, W. Knorr, P. P. Tans, J. W. C. White, and I. Levin (2003b), A comprehensive global three-dimensional model of δ^{18}O in atmospheric CO$_2$: 2. Mapping the atmospheric signal, *J. Geophys. Res.*, *108*(D17), 4528, doi:10.1029/2002JD003154.

Dansgaard, W. (1964), Stable isotopes in precipitation, *Tellus*, *16*, 436–468.

Dole, M. (1935), The relative atomic weight of oxygen in water and in air, *J. Am. Chem. Soc.*, *57*, 2731.

Dongmann, G. (1974), The contribution of land photosynthesis to the stationary enrichment of ^{18}O in the atmosphere, *Radiat. Environ. Biophys.*, *11*, 219–225.

Duplessy, J.-C., L. Labeyrie, A. Juillet-Leclerc, F. Maitre, J. Duprat, and M. Sarnthein (1991), Surface salinity reconstruction of the North Atlantic Ocean during the Last Glacial Maximum, *Oceanol. Acta*, *14*(4), 311–324.

Eppley, R. W., and B. J. Peterson (1979), Particulate organic matter flux and planktonic new production in the deep ocean, *Nature*, *282*, 677–680.

Farquhar, G. D., S. von Caemmerer, and J. A. Berry (1980), A biochemical model of photosynthetic CO$_2$ assimilation in leaves of C3 species, *Planta*, *149*, 78–90.

Farquhar, G. D., K. T. Hubick, A. G. Condon, and R. A. Richards (1989), Carbon isotope fractionation and plant water-use efficiency, in *Stable Isotopes in Ecological Research*, edited by P. W. Rundel, Springer-Verlag, New York.

Farquhar, G. D., J. Lloyd, J. A. Taylor, L. B. Flanagan, J. P. Syvertsen, K. T. Hubick, S. C. Wong, and J. R. Ehleringer (1993), Vegetation effects on the isotope composition of oxygen in atmospheric CO$_2$, *Nature*, *363*, 439–443.

Field, C. B., J. T. Randerson, and C. M. Malmstroem (1995), Global net primary production: Combining ecology and remote sensing, *Remote Sens. Environ.*, *51*, 74–88.

Förstel, H. (1978), The enrichment of ^{18}O in leaf water under natural conditions, *Radiat. Environ. Biophys.*, *15*, 323–344.

Friedlingstein, P., C. Delire, J.-F. Muller, and J.-C. Gerard (1992), The climate induced variation of the continental biosphere: A model simulation of the Last Glacial Maximum, *Geophys. Res. Lett.*, *19*, 897–900.

Friedlingstein, P., I. Fung, E. Holland, J. John, G. G. Brasseur, D. Erickson, and D. Schimel (1995a), On the contribution of the biospheric CO$_2$ fertilization to the missing sink, *Global Biogeochem. Cycles*, *9*, 541–556.

Friedlingstein, P., K. C. Prentice, I. Y. Fung, J. G. John, and G. P. Brasseur (1995b), Carbon-biosphere climate interactions in the Last Glacial Maximum climate, *J. Geophys. Res.*, *100*(D4), 7203–7222.

Gillon, J., and D. Yakir (2001), Influence of carbonic anhydrase activity in terrestrial vegetation on the ^{18}O content of atmospheric CO$_2$, *Science*, *291*, 2584–2587.

Guy, R. D., M. L. Fogel, and J. A. Berry (1993), Photosynthetic fractionation of the stable isotopes of oxygen and carbon, *Plant Physiol.*, *101*, 37–47.

Hansen, J. E., G. Russell, D. Rind, P. Stone, A. Lacis, S. Lebedeff, R. Ruedy, and L. Travis (1983), Efficient three-dimensional global models for climate studies: Model I and model II, *Mon. Weather Rev.*, *111*, 609–662.

Haxeltine, A., and I. C. Prentice (1996), BIOME3: An equilibrium terrestrial biosphere model based on ecophysiological constraints, resource availability, and competition among plant functional types, *Global Biogeochem. Cycles*, *10*(4), 693–709.

Hoffmann, G., M. Werner, and M. Heimann (1998), The water isotope module of the ECHAM atmospheric general circulation model: A study on timescales from days to several years, *J. Geophys. Res.*, *103*, 16,871–16,896.

Hoffmann, G., V. Masson, and J. Jouzel (2000), Stable water isotopes in atmospheric general circulation models, *Hydrol. Processes*, *14*, 1385–1406.

International Atomic Energy Agency (1992), Statistical treatment of data on environmental isotopes in precipitation, report, Vienna.

Jouzel, J., G. L. Russell, R. J. Suozzo, R. D. Koster, J. W. C. White, and W. S. Broecker (1987), Simulations of the HDO and ^{18}O atmospheric cycles using the NASA GISS general circulation model: The seasonal cycle for present-day conditions, *J. Geophys. Res.*, *92*, 14,739–14,760.

Jouzel, J., R. D. Koster, R. J. Suozzo, G. L. Russsel, J. W. C. White, and W. S. Broecker (1991), Simulations of the HDO and ^{18}O atmospheric cycles using the NASA GISS GCM: Sensitivity experiments for present-day conditions, *J. Geophys. Res.*, *96*, 7495–7507.

Jouzel, J., G. Hoffmann, F. Parrenin, and C. Waelbroeck (2002), Atmospheric oxygen 18 and sea-level changes, *Quat. Sci. Rev.*, *21*(1–3), 307–314.

Kaduk, J. (1996), Simulation der Kohlenstoffdynamik der globalen Landbiosphäre mit SILVAN -Modellbeschreibung und Ergebnisse., dissertation thesis, Univ. Hamburg, Hamburg.

Kaduk, J., and M. Heimann (1996), Assessing the climate sensitivity of the global terrestrial carbon cycle model SILVAN, *Phys. Chem. Earth*, *21*(5–6), 529–535.

Keeling, C. D. (1960), The concentration and isotopic abundances of carbon dioxide in the atmosphere, *Tellus*, *12*(2), 200–203.

Keeling, R. F. (1995), The atmospheric oxygen cycle: The oxygen isotopes of atmospheric CO$_2$ and O$_2$ and the N$_2$/O$_2$ ratio, *Rev. Geophys.*, 1253–1262.

Kiddon, J., M. L. Bender, J. Orchado, D. A. Caron, J. C. Goldman, and M. Dennett (1993), Isotopic fractionation of oxygen by respiring marine organisms, *Global Biogeochem. Cycles*, 7, 679–694.

Kim, J., and S. B. Verma (1991), Modelling canopy photosynthesis: Scaling up from a leaf to canopy in a temperate grassland ecosystem, *Agric. For. Meteorol.*, 57, 187–208.

Kroopnick, P. M. (1987), Oxygen 18 in dissolved oxygen, in *GEOSECS Atlantic, Pacific and Indian Ocean Expeditions*, edited by G. Oestlund et al., pp. 27–182, U.S. Gov. Printing Off., Washington, D. C.

Leuenberger, M. (1997), Modeling the signal transfer of seawater $\delta^{18}O$ to the $\delta^{18}O$ of atmospheric oxygen using a diagnostic box model for the terrestrial and marine biosphere, *J. Geophys. Res.*, 102, 26,841–26,850.

Lloyd, J., and G. D. Farquhar (1994), ^{13}C discrimination during CO_2 assimilation by the terrestrial biosphere, *Oecologia*, 99, 201–215.

Maier-Reimer, E. (1993), Geochemical cycles in an ocean general circulation model: Preindustrial tracer distributions, *Global Biogeochem. Cycles*, 7, 645–677.

Maier-Reimer, E., U. Mikolajewicz, and K. Hasselmann (1993), Mean circulation of the Hamburg LSG OGCM and its sensitivity to the thermohaline forcing, *J. Phys. Oceanogr.*, 23, 731–757.

Malaize, B., D. Paillard, J. Jouzel, and D. Raynaud (1999), The Dole effect over the last two Glacial-Interglacial cycles, *J. Geophys. Res.*, 104(D12), 14,199–14,208.

Miller, J. B., D. Yakir, J. W. C. White, and P. P. Tans (1999), Measurements of $^{18}O/^{16}O$ in the soil-atmosphere CO_2 flux, *Global Biogeochem. Cycles*, 13(3), 761–774.

Modellbetreuungsgruppe (1994), The ECHAM3 atmospheric general circulation model, report, Max-Planck Inst. fuer Meteorol., Hamburg, Germany.

Morita, N., and T. Titani (1936), Über den Unterschied in der Isotopenzusammensetzung von Luft-und Wassersauerstoff, *Bull. Chem. Soc. Jpn.*, 11, 36–38.

Najjar, R. G. (1990), Simulations of the phosphorus and oxygen cycles in the world ocean using a general circulation model, Ph.D. thesis, Princeton Univ., Princeton, N. J.

Olson, J. S., J. A. Watts, and L. J. Allison (1985), Major world ecosystem complexes ranked by carbon in live vegetation: A database, report, Oak Ridge Natl. Lab., Oak Ridge, Tenn.

Peylin, P., P. Ciais, A. S. Denning, P. P. Tans, J. A. Berry, and J. W. C. White (1999), A 3-dimensional study of $\delta^{18}O$ in atmospheric CO_2: Contribution of different land ecosystems, *Tellus, Ser. B*, 51, 642–667.

Prentice, I. C., M. T. Sykes, W. Cramer, R. A. Monserud, and A. M. Solomon (1992), A global biome model based on plant physiology and dominance, soil properties and climate, *J. Biogeogr.*, 19, 117–134.

Quay, P. D., S. Emerson, D. O. Wilbur, C. Stump, and M. Knox (1993), The $\delta^{18}O$ of dissolved O_2 in the surface waters of the subartic Pacific: A tracer of biological productivity, *J. Geophys. Res.*, 98(C5), 8447–8458.

Riley, W. J., C. J. Still, M. S. Torn, and J. A. Berry (2002), A mechanistic model of $H_2^{18}O$ and $C^{18}OO$ fluxes between ecosystems and the atmosphere: Model description and sensitivity analyses, *Global Biogeochem. Cycles*, 16(4), 585–598.

Robinson, S. A., D. Yakir, M. Ribas-Carbo, L. Giles, C. B. Osmond, J. N. Siedow, and J. A. Berry (1992), Measurements of the engagement of cyanide-resistant respiration in the Crassulacean acid metabolism plant Kalanchoe daigremontiana with the use of on-line oxygen isotope discrimination, *Plant Physiol.*, 100, 1087–1091.

Rozanski, K., L. Araguas-Araguas, and R. Gonfantini (1992), Relation between long-term trends of oxygen-18 isotope composition of precipitation and climate, *Science*, 258, 981–985.

Schmidt, G. A. (1999), Forward modeling of carbonate proxy data from planktonic foraminifera using oxygen isotope tracers in a global ocean model, *Paleoceanography*, 14(4), 482–497.

Seibt, U. (1997), Simulation der $^{18}O/^{16}O$-Zusammensetzung von atmosphärischen Sauerstoff, diploma thesis, Eberhard-Karls-Universität, Tübingen, Germany.

Seibt, U. (2003), Processes controlling the isotopic composition of CO_2 and O_2 in canopy air: A theoretical analysis with some observations in a Sitka spruce plantation, Ph.D. thesis, Univ. Hamburg, Hamburg, Germany.

Shackleton, N. J. (2000), The 100,000-year ice-age cycle identified and found to lag temperature, carbon dioxide, and orbital eccentricity, *Science*, 289, 1897–1902.

Shea, D. J. (1986), *Climatological Atlas: 1950–79*, Natl. Cent. for Atmos. Res., Boulder, Colo.

Six, K. D., and E. Maier-Reimer (1996), Effects of plankton dynamics on seasonal carbon fluxes in an ocean general circulation model, *Global Biogeochem. Cycles*, 10(4), 559–583.

Sowers, T., M. Bender, D. Raynaud, Y. S. Korotkevich, and J. Orchado (1991), The ^{18}O of atmospheric O_2 from air inclusions in the Vostok Ice Core: Timing of CO_2 and ice volume changes during the penultimate deglaciation, *Paleoceanography*, 6(6), 679–696.

von Caemmerer, S. (2000), *Biochemical Models of Leaf Photosynthesis*, Commonwealth Sci. and Ind. Res. Org., Collingwood, Australia.

Wang, X. F., and D. Yakir (1995), Temporal and spatial variations in the oxygen-18 content of leaf water in different plant species, *Plant Cell Environ.*, 18, 1377–1385.

Weber, C. (1996), Zur Dynamik des interhemisphärischen CO_2-Transports im Ozean, diploma thesis, Univ. Hamburg, Hamburg.

––––––––––––––––––

P. Ciais, M. Cuntz, P. Friedlingstein, G. Hoffmann, and J. Jouzel, Laboratoire des Sciences du Climat et de l'Environnement (LSCE), Orme des Merisiers, 91191 Gif sur Yvette, France. (ciais@lsce.saclay.cea.fr; cuntz@lsce.saclay.dea.fr; friedlingstein@lsce.saclay.cea.fr; hoffman@lsce.saclay.cea.fr; jouzel@lsce.saclay.cea.fr)

M. Heimann and U. Seibt, Max-Planck-Institut für Biogeochemie, Postfach 100164, D-07701 Jena, Germany. (martin.heimann@bgc-jena.mpg.de; seibt@bgc-jena.mpg.de)

J. Kaduk, Department of Geography, University of Leicester, Leicester LE1 7RH, UK. (j.kaduk@leicester.ac.uk)

E. Maier-Reimer, K. Six, and C. Weber, Max-Planck-Institut für Meteorologie, Bundesstrasse 55, D-20146 Hamburg, Germany. (maier-reimer@dkrz.de; six@dkrz.de; weber@dkrz.de)